JPE 14-1-11

http://dx.doi.org/10.6113/JPE.2014.14.1.105
ISSN(Print): 1598-2092 / ISSN(Online): 2093-4718

Current Sliding Mode Control with a Load Sliding Mode Observer for Permanent Magnet Synchronous Machines

Ningzhi Jin†, Xudong Wang*, and Xiaogang Wu*

†*Dept. of Electrical Engineering, Harbin University of Science and Technology, Harbin, China

Abstract

The sliding mode control (SMC) strategy is applied to a permanent magnet synchronous machine vector control system in this study to improve system robustness amid parameter changes and disturbances. In view of the intrinsic chattering of SMC, a current sliding mode control method with a load sliding mode observer is proposed. In this method, a current sliding mode control law based on variable exponent reaching law is deduced to overcome the disadvantage of the regular exponent reaching law being incapable of approaching the origin. A load torque-sliding mode observer with an adaptive switching gain is introduced to observe load disturbance and increase the minimum switching gain with the increase in the range of load disturbance, which intensifies system chattering. The load disturbance observed value is then applied to the output side of the current sliding mode controller as feed-forward compensation. Simulation and experimental results show that the designed method enhances system robustness amid load disturbance and effectively alleviates system chattering.

Keywords: Permanent magnet synchronous machine, Sliding mode control, Sliding mode observer

I. INTRODUCTION

The permanent magnet synchronous motor (PMSM) is a multivariable, nonlinear, and strong-coupled system that is extremely sensitive to parameters and disturbances; thus, its static and dynamic processes cannot be accurately described by traditional linear control methods, and its high operation performance is difficult to guarantee in a wide speed range [1], [2].

Sliding mode control (SMC) is a special nonlinear control method with advantages such as quick response, strong robustness, and simple implementation. However, this control method inevitably increases frequency chattering, thus making current research on the application of SMC to actual motor drive systems focus on how to alleviate chattering [3]-[6]. Current methods that effectively weaken system chattering applied to PMSM include boundary layer [7], [8], integral sliding surface [9],[10], reaching law [11]-[14], sliding mode observer [15]-[19], and intelligent control methods [20]-[22].

Exponent reaching law can obtain a quick response and weaken chattering, but its sliding motion area does not decay with time; that is, system states cannot reach the origin, whereas chattering does. The high-frequency components in the system model are excited, and the burden on the controller is consequently increased [11]. In [12], an SMC method based on the exponent reaching law was applied to the speed regulator of a PMSM vector control system; the method enhanced system robustness and the dynamic characteristics effectively. A variable-rate reaching law was proposed in [13], [14]; switching gain was designed as the product of a constant item and the state variable. The design solves the problem of the regular exponent reaching law being incapable of approaching the origin. However, when the system state arrives at the sliding band, system chattering remains high. To solve this problem, an improved exponent reaching law with time-varying switching gain is proposed in this study; that is, a modified factor with a small value and convergence to zero is introduced to switching gain to obtain minimal chattering on the arrival of the sliding band and to approach the origin finally.

In the SMC system, only the minimum switching gain that increases with the increase in the range of load disturbances can

Manuscript received Jul. 16, 2013; revised Oct. 17, 2013
Recommended for publication by Associate Editor Dong-Hee Lee.
†Corresponding Author: sharon0716@126.com
Tel: +86-0451-86390352, Fax: +86-0451-86390355, Harbin Univ. of Sci. & Tech.
*Dept. of Electrical Engineering, Harbin University of Science and Technology, China

meet the sliding mode existence and accessibility condition and thus resist the load disturbance effectively. However, an increase in switching gain intensifies system chattering. If the load observer method is introduced to compensate for the load disturbance, the value of switching gain will decrease significantly and system chattering will be greatly reduced. The regular open-loop load observer has a simple structure but does not use the output observation error for feedback correction of the load observed value; thus, the observer cannot guarantee its convergence and speed [15]. The regular closed-loop load observer can ensure the asymptotic stability of observation but depends on the cumbersome on-line identification of uncertain or time-varying parameters [16], [17]. A load observer based on sliding mode method can effectively inhibit the influence of parameter perturbations and load disturbances on system characteristics; however, reports on how to alleviate the chattering of the observed value are rare [18], [19]. To solve this problem, an improved extended load sliding mode observer is proposed in this study with load torque and speed as observed objects. An integral sliding surface with integral separation with respect to the speed observation error is adopted to avoid saturation. Switching gain is adjusted by the load disturbance observation error and is thus made convergent to zero. The designed observer can effectively weaken the chattering of the observed objects on the premise of the assurance of system robustness.

II. MATHEMATICAL MODEL OF PMSM

The stator voltage of PMSM in the d–q synchronous rotating reference frame can be expressed as

$$\begin{cases} u_{\mathrm{d}} = R_{\mathrm{s}} i_{\mathrm{d}} + L_{\mathrm{d}} \dfrac{\mathrm{d}i_{\mathrm{d}}}{\mathrm{d}t} - L_{\mathrm{q}} \omega_{\mathrm{e}} i_{\mathrm{q}} \\ u_{\mathrm{q}} = R_{\mathrm{s}} i_{\mathrm{q}} + L_{\mathrm{q}} \dfrac{\mathrm{d}i_{\mathrm{q}}}{\mathrm{d}t} + L_{\mathrm{d}} \omega_{\mathrm{e}} i_{\mathrm{d}} + \omega_{\mathrm{e}} \psi_{\mathrm{f}} \end{cases}, \tag{1}$$

where u_{d} and u_{q} are the d–q axis stator voltages, i_{d} and i_{q} are the d–q axis stator currents, L_{d} and L_{q} are the d–q axis inductances, R_{s} is the stator phase resistance, ψ_{f} is the rotor permanent magnet flux linkage, and ω_{e} is the rotor electrical angular speed.

The corresponding electromagnetic torque is

$$T_{\mathrm{e}} = 1.5 p(\psi_{\mathrm{f}} i_{\mathrm{q}} + (L_{\mathrm{d}} - L_{\mathrm{q}}) i_{\mathrm{d}} i_{\mathrm{q}}) . \tag{2}$$

The associated electromechanical equation is as follows:

$$T_{\mathrm{e}} - T_{\mathrm{L}} = J \frac{\mathrm{d}\omega_{\mathrm{m}}}{\mathrm{d}t} + B_{\mathrm{m}} \omega_{\mathrm{m}} , \tag{3}$$

where T_{L} is the load torque, p is the number of pole pairs, J is the moment of inertia, B_{m} is the friction coefficient, and ω_{m} is the rotor mechanical angular speed.

III. DESIGN OF CURRENT SMC

A. State Space Equation

In a current control system, the state variables are d–q axis current errors e_{d} and e_{q}, and the control inputs are d–q axis voltages u_{d} and u_{q}. Thus,

$$\begin{cases} \boldsymbol{x} = \begin{bmatrix} e_{\mathrm{d}} & e_{\mathrm{q}} \end{bmatrix}^{\mathrm{T}} = \begin{bmatrix} i_{\mathrm{dr}} - i_{\mathrm{d}} & i_{\mathrm{qr}} - i_{\mathrm{q}} \end{bmatrix}^{\mathrm{T}} \\ \boldsymbol{u} = \begin{bmatrix} u_{\mathrm{d}} & u_{\mathrm{q}} \end{bmatrix}^{\mathrm{T}} \end{cases}, \tag{4}$$

where i_{dr} and i_{qr} are the reference commands of the d–q axis currents.

The state space equation of the d–q axis current control system can be described from Eqs. (1) and (4) as

$$\begin{bmatrix} \dot{e}_{\mathrm{d}} \\ \dot{e}_{\mathrm{q}} \end{bmatrix} = \begin{bmatrix} A_1 & A_{12} \\ A_{21} & A_2 \end{bmatrix} \boldsymbol{x} + \begin{bmatrix} B_1 & 0 \\ 0 & B_2 \end{bmatrix} \boldsymbol{u} + \begin{bmatrix} E_1 \\ E_2 \end{bmatrix}, \tag{5}$$

where $A_1 = -\dfrac{R_{\mathrm{s}}}{L_{\mathrm{d}}}$, $A_{12} = \dfrac{L_{\mathrm{q}}}{L_{\mathrm{d}}} \omega_{\mathrm{e}}$, $A_{21} = -\dfrac{L_{\mathrm{d}}}{L_{\mathrm{q}}} \omega_{\mathrm{e}}$, $A_2 = -\dfrac{R_{\mathrm{s}}}{L_{\mathrm{q}}}$, $B_1 = -\dfrac{1}{L_{\mathrm{d}}}$, $B_2 = -\dfrac{1}{L_{\mathrm{q}}}$, $E_1 = \dfrac{R_{\mathrm{s}}}{L_{\mathrm{d}}} i_{\mathrm{dr}} - \dfrac{L_{\mathrm{q}}}{L_{\mathrm{d}}} \omega_{\mathrm{e}} i_{\mathrm{qr}}$, and $E_2 = \dfrac{L_{\mathrm{d}}}{L_{\mathrm{q}}} \omega_{\mathrm{e}} i_{\mathrm{dr}} + \dfrac{R_{\mathrm{s}}}{L_{\mathrm{q}}} i_{\mathrm{qr}} + \dfrac{1}{L_{\mathrm{q}}} \omega_{\mathrm{e}} \psi_{\mathrm{f}}$.

B. Sliding Surface

The integral sliding surface can eliminate static system errors and enhance control precision. Thus, the integral sliding surfaces with respect to the d–q axis current errors are utilized as follows:

$$\boldsymbol{s} = \begin{bmatrix} s_{\mathrm{d}} \\ s_{\mathrm{q}} \end{bmatrix} = \begin{bmatrix} c_1 \int_0^t e_{\mathrm{d}} \mathrm{d}t + e_{\mathrm{d}} \\ c_2 \int_0^t e_{\mathrm{q}} \mathrm{d}t + e_{\mathrm{q}} \end{bmatrix}, \tag{6}$$

where c_1 and c_2 are the integral coefficients of the d–q axis sliding surfaces.

C. Reaching Law

Given the disadvantage of the regular exponent reaching law, an improved exponent reaching law is proposed in this study, where a time-varying modified factor $\rho(|x|)$ is introduced to switching gain. The modified switching gain is then designed as the product of a constant item and $\rho(|x|)$.

Modified factor $\rho(|x|)$ is designed as follows:

$$\rho(|x|) = \frac{|x|}{|x| + \sigma_{\mathrm{d,q}}}, \tag{7}$$

where $\sigma_{\mathrm{d,q}}$ is the corresponding coefficient of either the d-axis or the q-axis modified factor. The reaching law with respect to the d–q axis current errors can then be expressed as

$$\dot{\boldsymbol{s}} = \begin{bmatrix} \dot{s}_{\mathrm{d}} \\ \dot{s}_{\mathrm{q}} \end{bmatrix} = \begin{bmatrix} -\varepsilon_1 \rho(|e_{\mathrm{d}}|)\mathrm{sgn}(s_{\mathrm{d}}) - \eta_1 s_{\mathrm{d}} \\ -\varepsilon_2 \rho(|e_{\mathrm{q}}|)\mathrm{sgn}(s_{\mathrm{q}}) - \eta_2 s_{\mathrm{q}} \end{bmatrix}, \tag{8}$$

where ε_1 and ε_2 are the switching gains of the d–q axis sliding surfaces and η_1 and η_2 are the exponent coefficients of the d–q axis sliding surfaces.

Therefore, modified switching gain $\varepsilon_1\rho(|e_{\mathrm{d}}|)$ or $\varepsilon_2\rho(|e_{\mathrm{q}}|)$ is always smaller than the original ε_1 or ε_2 and thus makes system chattering smaller upon arrival of the sliding band than the variable rate reaching law; it decays to zero with the system state to overcome the disadvantage of the regular exponent reaching law.

D. Control Law (Switching Function)

With E_1 and E_2 as disturbance terms, the current SMC law based on the improved exponent reaching law can be derived from Eqs. (4) to (8) as follows:

$$\boldsymbol{u} = \begin{bmatrix} u_{\mathrm{d}} \\ u_{\mathrm{q}} \end{bmatrix} = \begin{bmatrix} -\dfrac{1}{B_1}\left[(c_1 + A_1)e_{\mathrm{d}} + A_{12}e_{\mathrm{q}} + \varepsilon_1\rho(|e_{\mathrm{d}}|)\mathrm{sgn}(s_{\mathrm{d}}) + \eta_1 s_{\mathrm{d}}\right] \\ -\dfrac{1}{B_2}\left[(c_2 + A_2)e_{\mathrm{q}} + A_{21}e_{\mathrm{d}} + \varepsilon_2\rho(|e_{\mathrm{q}}|)\mathrm{sgn}(s_{\mathrm{q}}) + \eta_2 s_{\mathrm{q}}\right] \end{bmatrix}. \tag{9}$$

E. Continuous Switching Function

The sign functions in the control law in Eq. (9) can be replaced by a continuous smoothing function to alleviate the high-frequency chattering caused by sliding mode switching.

$$\mathrm{sgn}(s_{\mathrm{d,q}}) \approx \frac{s_{\mathrm{d,q}}}{|s_{\mathrm{d,q}}| + \delta_{\mathrm{d,q}}}, \tag{10}$$

where $\delta_{\mathrm{d,q}}$ is the smoothing coefficient of either the d-axis or the q-axis smoothing function. Chattering cannot be alleviated effectively if $\delta_{\mathrm{d,q}}$ is too small; otherwise, the dynamic responses of the sliding motion will worsen. Thus, these two conditions should be weighed to select an appropriate value of $\delta_{\mathrm{d,q}}$.

F. Stability Analysis

According to Lyapunov's stability theory, the sliding mode existence and accessibility condition is expressed as

$$\dot{V}(x) = \boldsymbol{s}^{\mathrm{T}}\dot{\boldsymbol{s}} < 0. \tag{11}$$

Substituting Eqs. (4) to (8) into Eq. (11) yields

$$\varepsilon_1 > |E_1| \quad \text{and} \quad \varepsilon_2 > |E_2|. \tag{12}$$

The minimum switching gain that increases only with the increase in the range of load disturbance can meet Eq. (12). However, the increase in switching gain intensifies system chattering. If the load observer method is introduced to compensate for the load disturbance, a small switching gain can meet the sliding mode existence and accessibility condition and thus weaken system chattering.

IV. Design of the Load Sliding Mode Observer

A. Extended State Space Equation

With electrical angular speed ω_{e} and load torque T_{L} as the state variables, electromechanical torque as the system input, and ω_{e} as the system output, the extended state space equation can be described from Eq. (3) as

$$\begin{cases} \begin{bmatrix} \dot{\omega}_{\mathrm{e}} \\ \dot{T}_{\mathrm{L}} \end{bmatrix} = \begin{bmatrix} -B_m J^{-1} & -pJ^{-1} \\ 0 & 0 \end{bmatrix}\begin{bmatrix} \omega_{\mathrm{e}} \\ T_{\mathrm{L}} \end{bmatrix} + \begin{bmatrix} pJ^{-1} \\ 0 \end{bmatrix} T_{\mathrm{e}} \\ \omega_{\mathrm{e}} = \begin{bmatrix} 1 & 0 \end{bmatrix}\begin{bmatrix} \omega_{\mathrm{e}} \\ T_{\mathrm{L}} \end{bmatrix} \end{cases}. \tag{13}$$

B. Observer Model

With speed ω_{e} and load torque T_{L} as the observed objects, the model of the load sliding mode observer is established from Eq. (13) as follows:

$$\begin{bmatrix} \dot{\hat{\omega}}_{\mathrm{e}} \\ \dot{\hat{T}}_{\mathrm{L}} \end{bmatrix} = \begin{bmatrix} -\dfrac{B_{\mathrm{m}}}{J} & -\dfrac{p}{J} \\ 0 & 0 \end{bmatrix}\begin{bmatrix} \hat{\omega}_{\mathrm{e}} \\ \hat{T}_{\mathrm{L}} \end{bmatrix} + \begin{bmatrix} \dfrac{p}{J} \\ 0 \end{bmatrix} T_{\mathrm{e}} + \begin{bmatrix} 1 \\ l \end{bmatrix} f(\omega_{\mathrm{e}} - \hat{\omega}_{\mathrm{e}}), \tag{14}$$

where l is the feedback gain of the observer and $f(\omega_{\mathrm{e}} - \hat{\omega}_{\mathrm{e}})$ represents the sliding mode control function with respect to observation error $\omega_{\mathrm{e}} - \hat{\omega}_{\mathrm{e}}$, which depends on its sliding surface and reaching law.

Subtracting Eq. (14) from Eq. (13) yields the error equation of the observer.

$$\begin{cases} \dot{e}_{\omega} = -\dfrac{B_{\mathrm{m}}}{J}e_{\omega} - \dfrac{p}{J}e_{\mathrm{T}} - f(e_{\omega}) \\ \dot{e}_{\mathrm{T}} = -lf(e_{\omega}) \end{cases}, \tag{15}$$

where $e_{\omega} = \omega_{\mathrm{e}} - \hat{\omega}_{\mathrm{e}}$ and $e_{\mathrm{T}} = T_{\mathrm{L}} - \hat{T}_{\mathrm{L}}$.

C. Sliding Surface

The integral sliding surface can reduce static system errors but may result in saturation and even system oscillation. An integral separation-based integral sliding surface is designed in this study to solve this problem. The integral function is canceled to avoid saturation when system error e_{ω} is greater than preset threshold $e_{\omega(\mathrm{th})}$.

The integral sliding surface with integral separation with respect to the speed observation error can then be expressed as

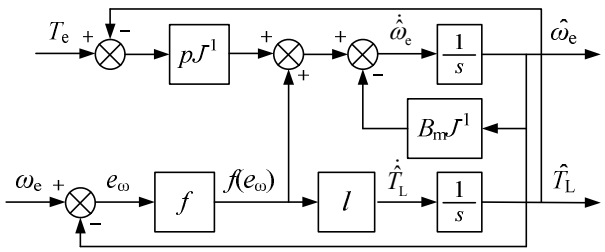

Fig. 1. Structural diagram of the load sliding mode observer.

$$s_\omega = \begin{cases} c_\omega \int_0^t e_\omega \mathrm{d}t + e_\omega & |e_\omega| < e_{\omega(\mathrm{th})} \\ e_\omega & |e_\omega| > e_{\omega(\mathrm{th})} \end{cases}, \tag{16}$$

where c_ω and $e_{\omega(\mathrm{th})}$ are the integral coefficient and the separation threshold of the observer integral sliding surfaces, respectively.

D. Reaching Law

The exponent reaching law with respect to the speed observation error can be expressed as

$$\dot{s}_\omega = c_\omega e_\omega + \dot{e}_\omega = -\varepsilon_\omega \operatorname{sgn}(s_\omega) - \eta_\omega s_\omega , \tag{17}$$

where ε_ω and η_ω are the switching gain and the exponent coefficient of the observer reaching law, respectively.

E. Control Law

By substituting Eq. (15) into Eq. (17) and with $-\frac{p}{J}e_T$ as the disturbance term, the sliding mode control law of the load sliding mode observer can be deduced as follows:

$$f(e_\omega)=(c_\omega - B_m J^{-1})e_\omega + \varepsilon_\omega \operatorname{sgn}(s_\omega) + \eta_\omega s_\omega . \tag{18}$$

Thus, the structure diagram of the load sliding mode observer can be generated according to Eqs. (13) to (18) as shown in Fig. 1.

F. Stability Analysis

According to Lyapunov's stability theory in Eq. (11), the sliding mode existence and accessibility condition of the load observer can be derived from Eqs. (14) to (18) as

$$\varepsilon_\omega > \frac{p}{J}|e_T| . \tag{19}$$

When load torque observation error e_T is large, necessary switching gain ε_ω and the resulting chattering of the observed objects are also large.

G. Switching Gain

To solve the problem above, a method that involves the on-line adjustment of switching gain is proposed in this study. Switching gain ε_ω is adaptively tuned by load torque observation error e_T. The designed observer can weaken the observed chattering on the premise of the assurance of system stability.

The adaptive adjustment law with respect to switching gain ε_ω is then designed as follows:

$$\varepsilon_\omega = k_\varepsilon \frac{p}{J}|e_T| , \tag{20}$$

where k_ε is a constant greater than 1. Thus, when load observation error e_T is large, switching gain ε_ω should also be large to ensure observer robustness; otherwise, when e_T converges to zero, ε_ω approaches zero and observation chattering decreases.

H. Load Compensation

Load disturbance observed value $\hat{T}_L$ is equivalently compensated to the output side of the current SMC to reduce switching gain in the control law in Eq. (9); thus, we can obtain the current SMC law with load torque feed-forward compensation as follows:

$$\boldsymbol{u}' = \begin{bmatrix} u'_d \\ u'_q \end{bmatrix} = \begin{bmatrix} -\frac{1}{B_1}\left[(c_1 + A_1)e_d + A_{12}e_q + \varepsilon_1 \rho(|e_d|)\operatorname{sgn}(s_d) + \eta_1 s_d + k_{cd}\hat{T}_L\right] \\ -\frac{1}{B_2}\left[(c_2 + A_2)e_q + A_{21}e_d + \varepsilon_2 \rho(|e_q|)\operatorname{sgn}(s_d) + \eta_2 s_q + k_{cq}\hat{T}_L\right] \end{bmatrix}, \tag{21}$$

where k_{cd} and k_{cq} are the load compensation coefficients of the d–q axis SMC law. In the motor mode ($i_q > 0$ and $i_d < 0$), items $-B_1^{-1}k_{cd}\hat{T}_L$ and $-B_2^{-1}k_{cq}\hat{T}_L$ are compensated for items $-L_q\omega_e i_q$ and $L_d\omega_e i_d + \omega_e\psi_f$ of stator voltages u_d and u_q in Eq. (1) separately. Therefore, $-B_1^{-1}k_{cd} < 0$ and $-B_2^{-1}k_{cq} > 0$.

Similarly, according to Lyapunov's stability theory in Eq. (11), the stability condition of the current SMC can be deduced from Eqs. (4) to (8) as

$$\varepsilon_1 > \left|E_1 - k_{cd}\hat{T}_L\right| \text{ and } \varepsilon_2 > \left|E_2 - k_{cq}\hat{T}_L\right| . \tag{22}$$

Adopting the load torque compensation method significantly reduces switching gain and thus effectively alleviates system chattering.

V. Simulation Results and Analysis

A simulation model of the PMSM drive and control system (Fig. 2) is built and examined in MATLAB.

The PI control method is applied to the speed outer loop in the system model. The speed controller provides current command i_{sr}, which is distributed in d–q axis current commands i_{dr} and i_{qr} according to the maximum torque per ampere vector control rule. The improved exponent reaching

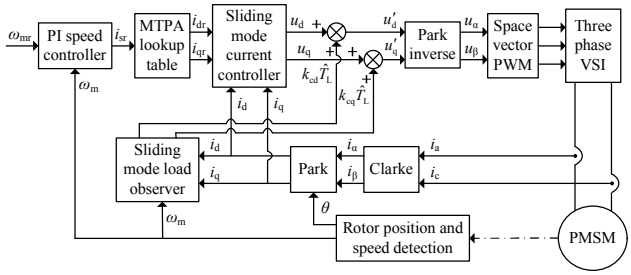

Fig. 2. Structural diagram of the system simulation model.

TABLE I
PARAMETERS OF THE CURRENT SMC AND LOAD SLIDING MODE OBSERVER

Parameters	Values
$-B_1^{-1}\varepsilon_1$, $-B_2^{-1}\varepsilon_2$	185.0, 175.0
σ_d , σ_q	6.0, 3.0
$-B_1^{-1}c_1$, $-B_2^{-1}c_2$	0.03, 0.05
k_ε	1.5
c_ω , $e_{\omega(th)}$	0.12, 50
$-B_1^{-1}k_{cd}$, $-B_2^{-1}k_{cq}$	-1.5, 1.4

law based on the SMC method is employed in the current inner loop combined with the sliding mode observer based on the load disturbance compensation method to alleviate the system chattering of the SMC.

The main parameters of the designed current SMC in the simulation and experiments are shown in Table I. The sampling time of the controller is 100 μs in the simulation, similar to the switching time, and 2 ms (20 times the length of the switching time) in the experiments.

Figs. 3 and 4 show the simulation curves of the loading and unloading responses of the observed load torque under a speed command of 3000 r/min. The load torque abruptly changes from 36 N·m to 72 N·m at t=10.0 s and from 72 N·m to 36 N·m at t=20.0 s. Constant switching gain is employed in the regular method, whereas adaptive switching gain is applied in the improved load observation method as shown in Eq. (20). For the improved method, the observed load torque responds more quickly and has a smaller overshoot; thus, the improved load sliding mode observer has better tracking characteristics.

Figs. 5 and 6 provide comparisons of the simulation curves of the current tracking responses of step load in the regular, improved exponent reaching law, and improved load observation and compensation methods under a speed command of 3000 r/min. The load torque changes abruptly from 36 N·m to 72 N·m at t=10.0 s and from 72 N·m to 36 N·m at t=20.0 s. Constant switching gain is employed in the regular method without the load observer. The modified switching gain with the time-varying factor shown in Eq. (7) is applied to the improved exponent reaching law method

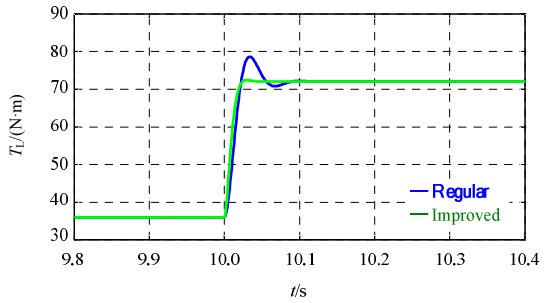

Fig. 3. Simulation curves of the loading responses of observed load torque.

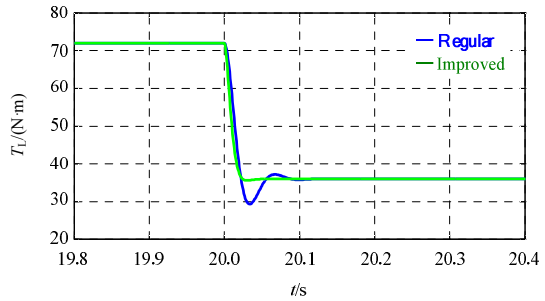

Fig. 4. Simulation curves of the unloading responses of observed load torque.

without the load observer, whereas the improved exponent reaching law with time-varying switching gain and the improved observer with the adaptive switching gain are both adopted in the improved load observation and compensation method. In the dynamic processes, the d–q axis currents for the improved reaching law method respond more quickly and have a smaller overshoot than the regular one, whereas those for the improved compensation method respond the quickest and have the smallest overshoot; thus, the designed SMC has superior current tracking characteristics with load disturbance. In the steady states, the d–q axis current ripples for the improved reaching law method are smaller than the regular one, whereas those for the improved compensation method are the smallest. This result is consistent with the theoretical analysis on the reaching law and observer in Sections III and IV.

VI. EXPERIMENTAL RESULTS AND ANALYSIS

Loading and unloading experiments are performed for the proposed reaching law and observer methods to validate the system characteristics of the anti-disturbance and chattering inhibition of the current SMC. The hardware configuration of the PMSM drive and control system is shown in Fig. 7. The related parameters of PMSM are shown in Table II.

Figs. 8 and 9 provide comparisons of the tracking responses with load change between the regular observer and the improved one under a speed command of 3000 r/min. The

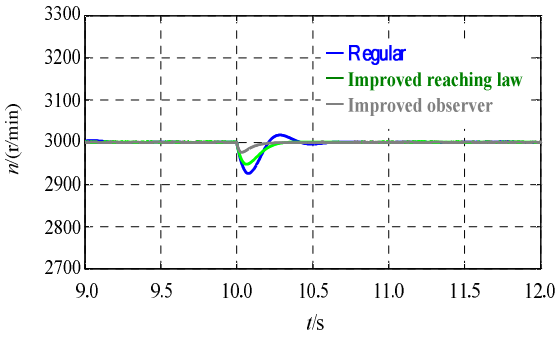

(a)

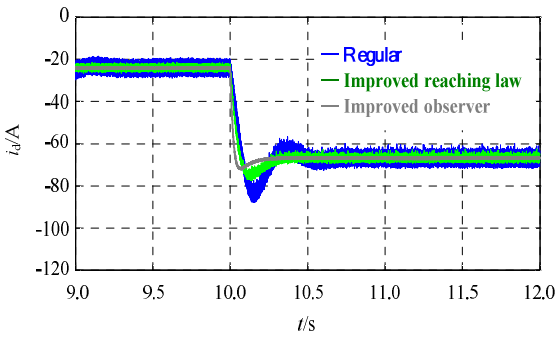

(b)

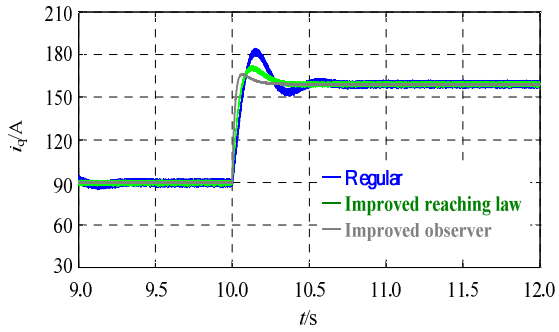

(c)

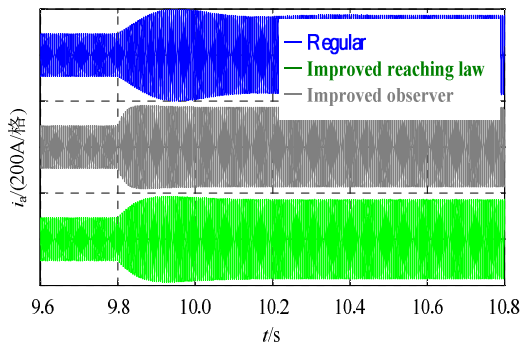

(d)

Fig. 5. Simulation curves of the loading current tracking responses. (a) Speed responses. (b) D-axis current responses. (c) Q-axis current responses. (d) Phase current responses.

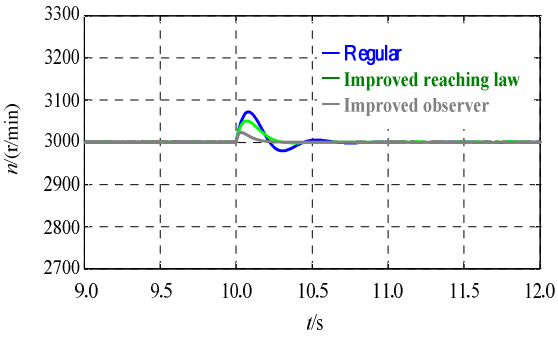

(a)

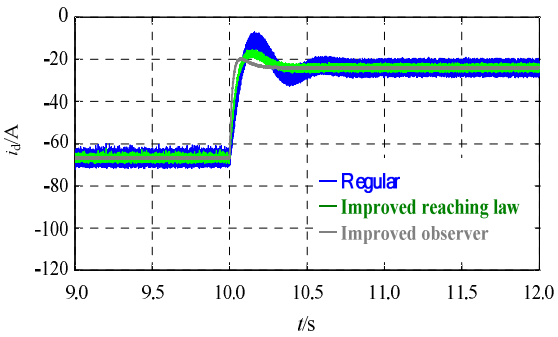

(b)

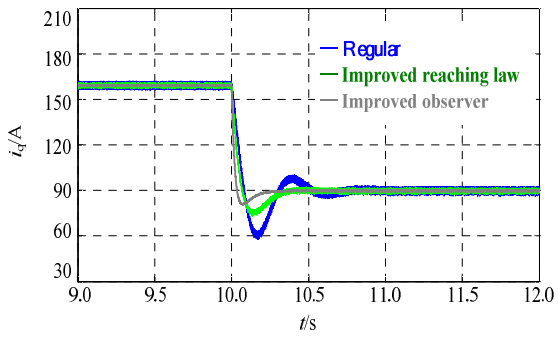

(c)

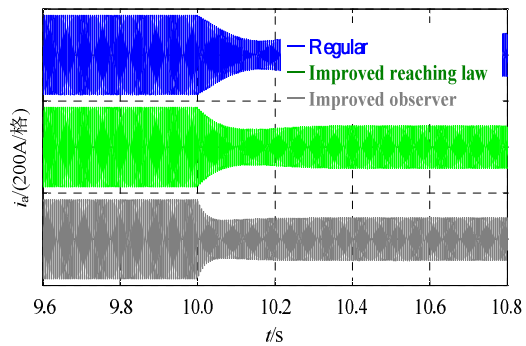

(d)

Fig. 6. Simulation curves of the unloading current tracking responses. (a) Speed responses. (b) D-axis current responses. (c) Q-axis current responses. (d) Phase current responses.

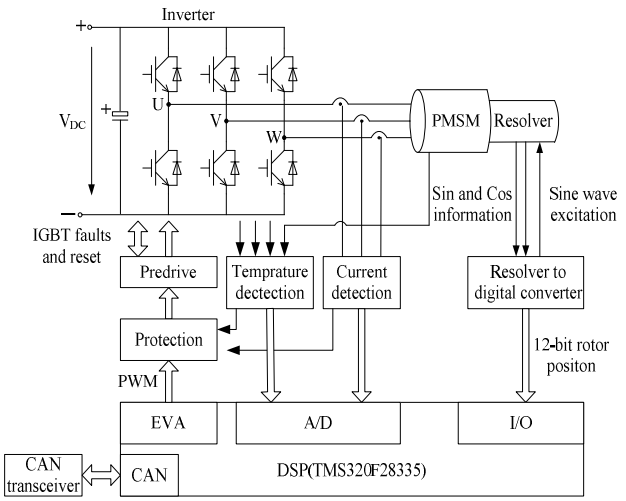

Fig. 7. Hardware configuration of the PMSM drive and control system.

TABLE II
PARAMETERS OF PMSM

Parameters	Values
Output power (kW)	30
Rated speed (r/min)	4500
Rated torque (N·m)	72
D-axis and Q-axis inductances (mH)	0.13 and 0.33
Flux linkage (Wb)	0.062
Number of pole pairs	4

load torque increases from 36 N·m to 72 N·m suddenly at t=10.0 s and decreases from 72 N·m to 36 N·m abruptly at t=10.4 s. The improved load torque observer responds more quickly and has no obvious overshoot; thus, the improved observation method has better tracking characteristics with load disturbance.

Figs. 10 and 11 provide comparisons of the current dynamic index with different step load changes, where ΔT_L represents a step change from a different load to the full load with a maximum value of $72-18=54(\mathrm{N\cdot m})$ in actual operating conditions. When the load torque provides a step change within the rated range, the overshoot for the regular method is approximately 30%; that for the improved reaching law method decreases to approximately 15% and that for the improved observer one decreases further to approximately 10%. The adjustment time for the regular method is approximately 490 ms, that for the improved reaching law one decreases to 360 ms, and that for the improved observer one decreases further to 220 ms.

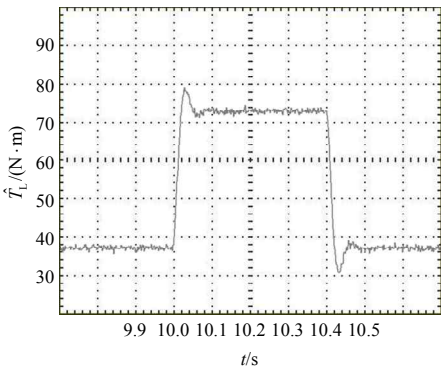

Fig. 8. Experimental curves of the tracking response with load change for the regular observer.

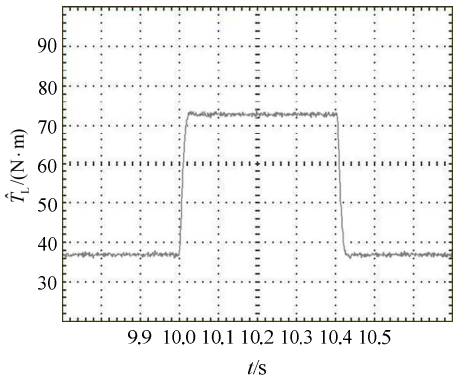

Fig. 9. Experimental curves of tracking response with load change for the improved observer.

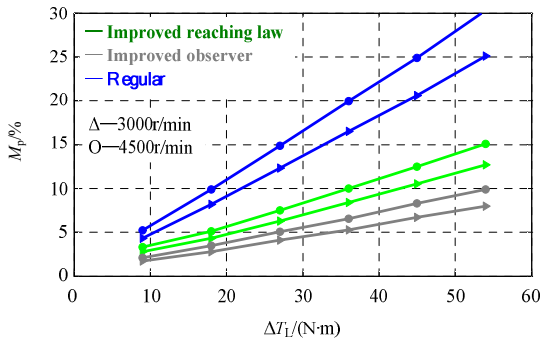

Fig. 10. Comparisons of current dynamic index–overshoot with step load.

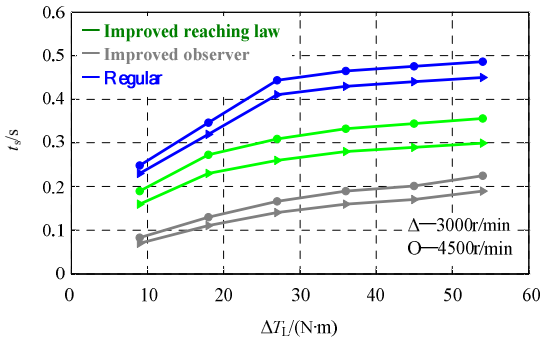

Fig. 11. Comparison of the current dynamic index–adjustment time with step load.

Figs. 12 to 14 provide comparisons of the loading responses of the regular method, improved exponent reaching law method, and improved load observation and compensation method under a speed command of 3000 r/min, where the load torque abruptly increases from 36 N·m to 72 N·m at t=10.0 s. Figs. 15 to 17 provide comparisons of the unloading responses of the three abovementioned methods under the same speed command, where the load torque abruptly decreases from 72 N·m to 36 N·m at t=20.0 s. The currents and speed for the improved reaching law method respond more quickly and exhibit less chattering in both the dynamic and static states than the regular one, whereas those for the improved compensation method respond the quickest and exhibit the least chattering. Therefore, the designed controller with a load observer enhances the system characteristics under load disturbance and alleviates system chattering significantly.

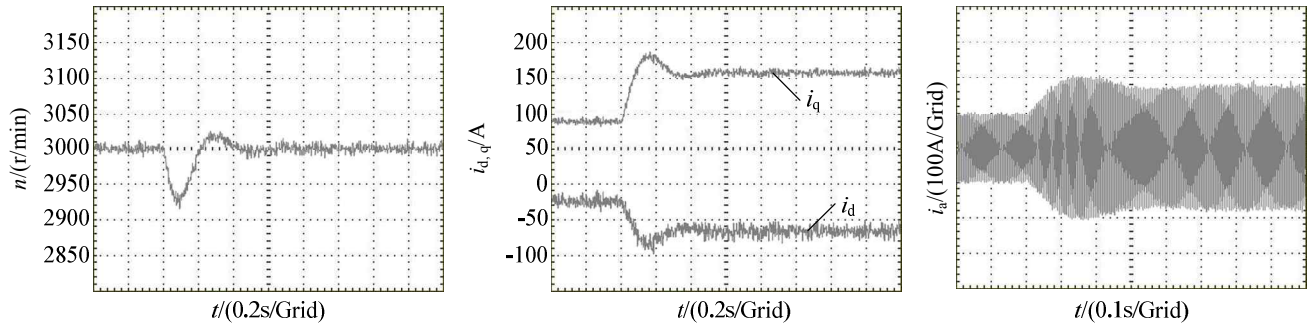

Fig. 12. Experimental curves of the loading responses for the regular method. (a) Speed response. (b) D–q axis current responses. (c) Phase current response.

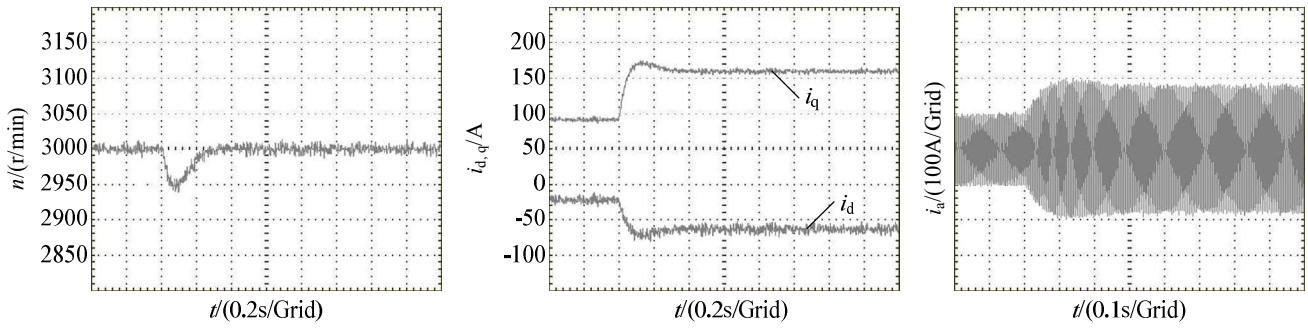

Fig. 13. Experimental curves of the loading responses for the improved reaching law method. (a) Speed response. (b) D–q axis current responses. (c) Phase current response.

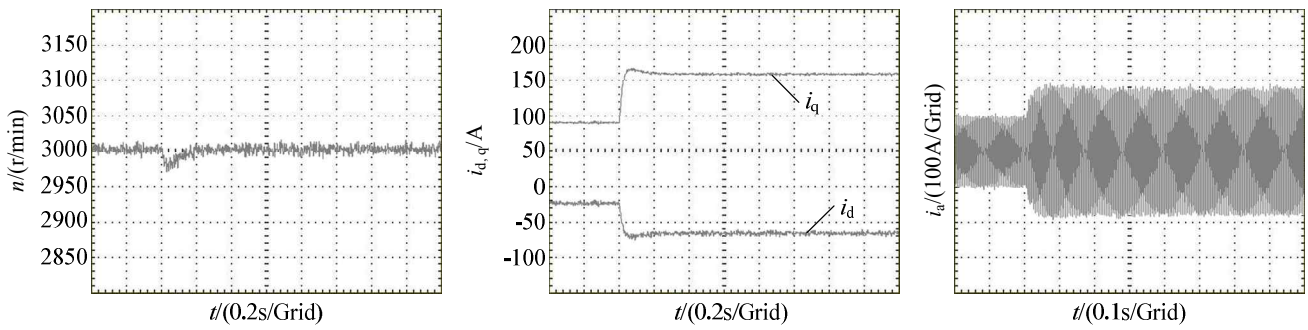

Fig. 14. Experimental curves of the loading responses for the improved load observer method. (a) Speed response. (b) D–q axis current responses. (c) Phase current response.

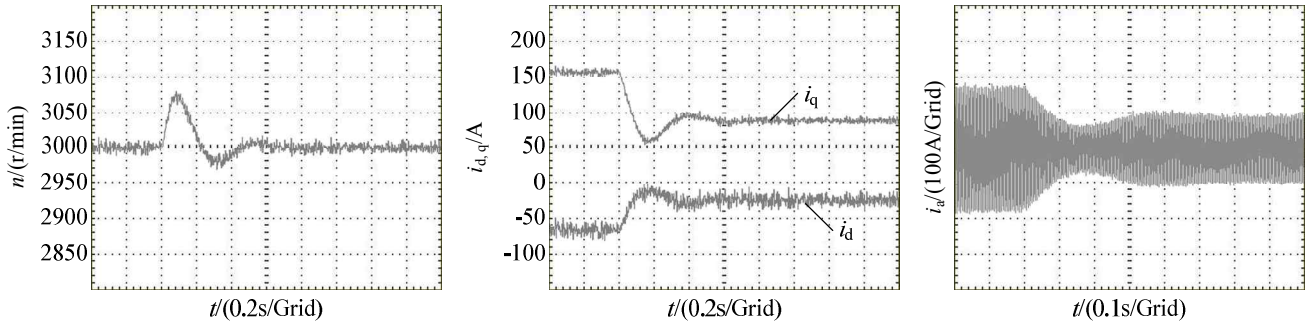

Fig. 15. Experimental curves of the unloading responses for the regular method. (a) Speed response. (b) D–q axis current responses. (c) Phase current response.

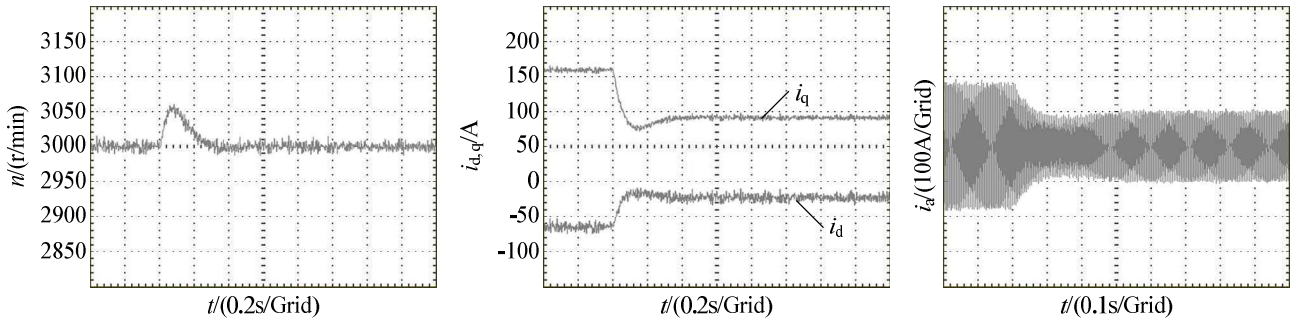

Fig. 16. Experimental curves of the unloading responses for the improved reaching law method. (a) Speed response. (b) D–q axis current responses. (c) Phase current response.

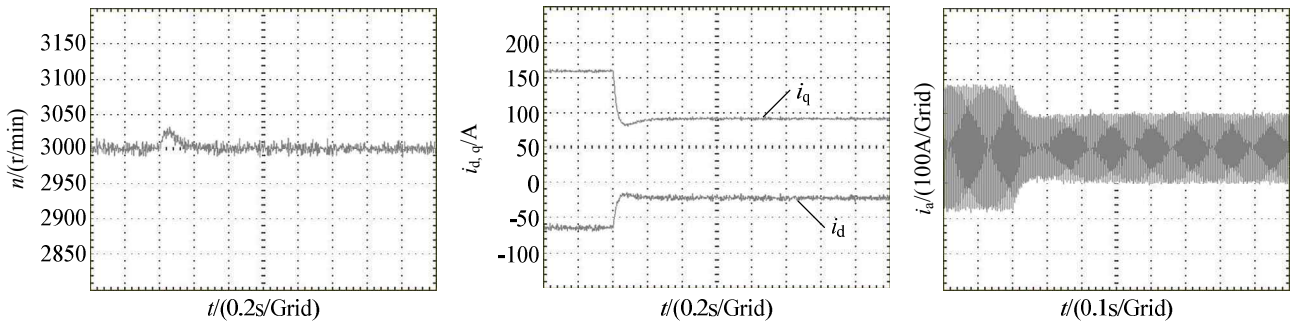

Fig. 17. Experimental curves of the unloading responses for the improved load observer method. (a) Speed response. (b) D–q axis current responses. (c) Phase current response.

VII. CONCLUSION

SMC has the advantages of quick response, strong robustness, and simple implementation. To improve system robustness amid parameter changes and disturbances, the SMC strategy was applied to the PMSM vector control system. However, this control strategy inevitably results in high-frequency chattering. In view of the problem of intrinsic chattering in the SMC system, a current SMC method with a load sliding mode observer was developed. In this method, an improved exponent reaching law based on the current SMC law was deduced. A load torque sliding mode observer model with adaptive switching gain was built, and the load disturbance observed value was compensated to the output side of the current SMC. Simulation and experimental results show that the designed SMC enhances system robustness amid load disturbance, alleviates system chattering effectively, and thus improves system static and dynamic characteristics under load disturbance.

ACKNOWLEDGEMENTS

This project is supported by the National Natural Science Foundation of China (No. 51177031) and the National High Technology Research and Development Program (863 Program) of China (No. SQ2010AA1122991001).

REFERENCES

[1] W. Cai, "Starting engines and powering electric loads with one machine," *IEEE Ind. Appl. Mag.*, Vol. 12, No. 6, pp. 29-38, Nov./Dec. 2006.
[2] Z. Q. Zhu and D. Howe, "Electrical machines and drives for electric, hybrid, and fuel cell vehicles," *Proceedings of the IEEE*, Vol. 95, No. 4, pp. 746-765, Apr. 2007.
[3] V. I. Utkin, *Sliding Modes in Control and Optimization*. Berlin: Springer-Verlag, chap. 7, 1992.
[4] C. F. Zhang, Y.N. Wang, and J. He, "Variable strcture intelligent control for PM synchronous servo motor drive," *Proceedings of the CSEE*, Vol. 22, No. 7, pp. 13-17, Jul. 2002.
[5] S. C. Fang, B. Zhou, J. J. Huang, and D. Li, "Sliding mode control for PMSM drive system," *Transanctions of China Electrotechnical Society*, Vol. 23, No. 8, pp. 29-35, Aug. 2008.
[6] H. P. Jia, D. Sun, and Y. K. He, "The PMSM DTC based on variable structure sliding mode," *Proceedings of the CSEE*, Vol. 26, No. 20, pp. 134-138, Oct. 2006.
[7] M. S. Chen, Y. R. Hwang, and M. Tomizuka, "A state-dependent boundary layer design for sliding mode control," *IEEE Transactions on Automatic Control*, Vol. 47, No. 10, pp. 1677-1681, Oct. 2002.
[8] V. Parra-Vega and G. Hirzinger, "Chattering-free sliding mode control for a class of nonlinear mechanical systems," *International Journal of Robust and Nonlinear Control*, Vol. 11, pp. 1161-1178, 2001.
[9] S. Seshagiri and H. K. Khalil, "On introducing integral action in sliding mode control," *in Proc. IEEE Conf. Decis. Control,* pp. 1473-1478, 2002.
[10] S. Seshagiri and H. K. Khalil, "Robust output feedback regulation of minimum-phase nonlinear aystems using conditional integrators," *Automatica*, Vol. 41, pp. 43-54, 2005.
[11] W. B. Gao, *Variable structure control theory and design method*. Beijing: Science Press, chap. 5, 1996.
[12] H. B. Wang, B. Zhou, and S. C. Fang, "A PMSM sliding mode control system based on exponential reaching law," *Transanctions of China Electrotechnical Society*, Vol. 24, No. 9, pp. 71-77, Sep. 2009.
[13] K. W. Tong, X. Zhang, Y. Zhang, Z. Xie, and R. X. Cao, "Sliding mode variable structure control of permanent magnet synchronous machine based on a novel reaching law," *Proceedings of the CSEE*, Vol. 28, No. 21, pp. 102-106, Jul. 2008.
[14] L. Z. Song, H. Wen, Q. C. Yao, "Sliding mode variable structure control of permanent magnet synchronous machine based on a novel reaching law," *Journal of Naval Academy of Engineering*, No. 3, pp. 16-21, 1999.
[15] Y. Liu, B. Zhou, and S. C. Fang, "Sliding mode control of PMSM based on a novel disturbance observer," *Proceedings of the CSEE,* Vol. 30, No. 9, pp. 80-85, Mar. 2010.
[16] W. Q. Lu, Y.W. Hu, J.Y. Liang and W. X. Huang, "Anti-disturbance adaptive control for permanent magnet synchronous motor servo system," *Proceedings of the CSEE,* Vol. 31, No. 3, pp. 75-81, Jan. 2011.
[17] V. Q. Leu, H. H. Choi, and J. W. Jung, "Fuzzy sliding mode speed controller for PM synchronous motors with a load torque observe," *IEEE Transactions on Power Electronics*, Vol. 27, No. 3, pp. 1530-1539, Mar. 2012.
[18] X. G. Zhang, L. Sun, and K. Zhao, "Sliding mode control of PMSM based on a novel load torque sliding mode observer," *Proceedings of the CSEE,* Vol. 32, No. 3, pp. 111-116, Jan. 2012.
[19] Z. Y. Wang, C. S. Wang, X. Qi, and X.M. Zhou, "Study on MRAS sliding-mode load torque observer based on PMSM," *Electric Machines and Control,* Vol. 16, No. 1, pp. 45-49, Jan. 2012.
[20] R. J. Wai, "Total sliding-mode controller for PM synchronous servo motor drive using recurrent fuzzy neural network," *IEEE Transactions on Industrial Electronics,* Vol. 48, No. 5, pp. 926-944, Oct. 2001.
[21] H. L. Xin, and J. B. Ho, "A new design method for gain-scheduling variable structure controllers ," *Control and Design,* Vol. 26, No. 12, pp. 1824-1828+1834, Dec. 2011

Ningzhi Jin was born in Harbin, China, in 1980. He received his B.S., M.S., and Ph.D. degrees in electrical engineering from Harbin University of Science and Technology, Harbin, China, in 2003, 2006, and 2012, respectively. He is a lecturer of power electronics and power drive in Harbin University of Science and Technology. His research interests include motor drive and power electronics.

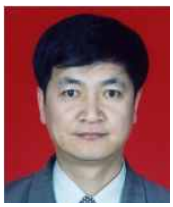

Xudong Wang was born in Jixi, China, in 1956. He received his B.S. and M.S. degrees in electrical engineering from the Harbin Institute of Electrical Engineering, Harbin, China, in 1982 and 1987, respectively, and his Ph.D. degree in mechanical electronics from the Harbin Institute of Technology, Harbin, China, in 2000. He is a professor and doctor supervisor of power electronics and power drive in Harbin University of Science and Technology. He has been the director of the Engineering Research Center of the Automotive Electronic Drive Control and System Integration of the Ministry of Education in China since 2006. His research interests include automotive electronics and the traction motors and drives of electric vehicles.

Xiaogang Wu was born in Harbin, China, in 1981. He received his B.S., M.S., and Ph.D. degrees in electrical engineering from Harbin University of Science and Technology, Harbin, China, in 2003, 2006, and 2009, respectively. He is an associate professor of power electronics and power drive in Harbin University of Science and Technology. His research interest is the power train control of electric vehicles.